

Nanoscale

Accepted Manuscript



This is an *Accepted Manuscript*, which has been through the Royal Society of Chemistry peer review process and has been accepted for publication.

Accepted Manuscripts are published online shortly after acceptance, before technical editing, formatting and proof reading. Using this free service, authors can make their results available to the community, in citable form, before we publish the edited article. We will replace this *Accepted Manuscript* with the edited and formatted *Advance Article* as soon as it is available.

You can find more information about *Accepted Manuscripts* in the [Information for Authors](#).

Please note that technical editing may introduce minor changes to the text and/or graphics, which may alter content. The journal's standard [Terms & Conditions](#) and the [Ethical guidelines](#) still apply. In no event shall the Royal Society of Chemistry be held responsible for any errors or omissions in this *Accepted Manuscript* or any consequences arising from the use of any information it contains.

ARTICLE

Graphitic Carbon Nitride Nanosheet @ Metal-Organic Framework Core-shell Nanoparticles for Photo-chemo Combination Therapy

Cite this: DOI: 10.1039/x0xx00000x

Rui Chen^a, Jinfeng Zhang^a, Yu Wang^a, Xianfeng Chen^{*b}, J. Antonio Zapien^a and Chun-Sing Lee^{*a}Received xxxx 2015,
Accepted xxxx 2015

DOI: 10.1039/x0xx00000x

www.rsc.org/Nanoscale

Recently, nanoscale metal-organic frameworks (NMOFs) start to be developed as a promising platform for bioimaging and drug delivery. On the other hand, combinational therapies using multiple approaches are demonstrated to achieve much enhanced efficacy. Herein, we report, for the first time, core-shell nanoparticles consisting of a photodynamic therapeutic (PDT) agent and MOF shell while simultaneously carrying chemotherapeutics drug for effective combinational therapy. In the work, core-shell nanoparticles of zeolitic-imidazole framework-8 (ZIF-8) as shell embedded with graphitic carbon nitride (g-C₃N₄) nanosheets as core are fabricated by growing ZIF-8 in the presence of g-C₃N₄ nanosheets. Doxorubicin hydrochloride (DOX) is then loaded into the ZIF-8 shell of the core-shell nanoparticles. The combination of the chemotherapeutic effects of DOX and the PDT effect of g-C₃N₄ nanosheets can lead to considerably enhanced efficacy. Furthermore, the red fluorescence of DOX and the blue fluorescence of g-C₃N₄ nanosheets provide additional function of dual-color imaging for monitoring the drug release process.

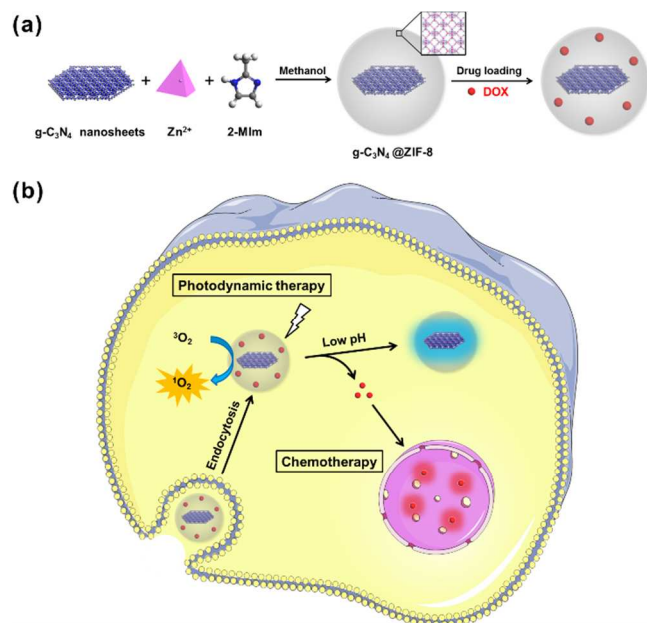
1. Introduction

Metal-organic frameworks (MOFs) are self-assemblies obtained by linking metal ions or clusters with bridging polydentate ligands and have attracted wide attention for their applications in gas storage¹⁻⁴, catalysis⁵⁻⁷, sensing^{8,9} and separation^{10,11} which stem from their high and tunable porosities and versatile functionalities.¹²⁻¹⁵ Besides, their inherent porosity endows nanoscale metal-organic frameworks (NMOFs) with fast diffusion channels which are beneficial to many applications.¹⁶ For example, this allows fast ion transport in high-rating lithium ion battery^{17,18} and efficient diffusion of reactive oxygen species (ROS) for photodynamic therapy¹⁹. In the past couple of decades, NMOFs have been highlighted as a promising delivery platform for biomedical applications.²⁰⁻²³ As a hybrid organic-inorganic nanomaterial, NMOFs possess many potent features such as high loading capacity, progressive biodegradability and low cytotoxicity²⁴, and are an ideal nanocarrier for delivery of anti-cancer drugs to tumor sites.²⁵⁻²⁷

On the other hand, there has been an emerging interest in combining therapeutic modalities to synergistically address diseases which cannot be easily handled with a single therapeutic approach.²⁸⁻³⁰ Notably, the combination of dual therapies such as chemo- and photodynamic therapy (PDT) has been demonstrated to provide improved efficacy, reduced side effects, and retarded multiple drug resistance (MDR).³¹⁻³⁵ As an example, Lin *et al.* have successfully synthesized nanoscale coordination polymer @ pyrolipid core-shell nanoparticles that

incorporate chemotherapeutics and photodynamic agents to achieve enhanced anti-tumor efficacy.³⁶

More recently, integrations of nanoparticles and NMOFs have been employed to build novel core-shell systems for catalyst³⁷⁻³⁹. On the other hand, there are rare reports of such systems for biomedical applications.^{40,41} Very recently, Lin *et al.* have reported up-conversion nanoparticles @ MOF nanocomposites as theranostic nanoplatform for up-conversion fluorescence imaging and drug delivery respectively.⁴⁰ Tang *et al.* have synthesized up-conversion nanoparticles @ Fe-MOFs core-shell nanoprobos for *in vivo* luminescent/magnetic dual-mode imaging.⁴¹ While NMOFs have been extensively used as carriers for imaging agents and drugs of different modalities, so far there is no report on exploiting the advantages of NMOFs for combinational therapy. In this work we prepared core-shell nanoparticles, each of which contains graphitic carbon nitride (g-C₃N₄) nanosheets encapsulated by a zeolitic-imidazole frameworks-8 (ZIF-8) shell (Scheme 1a). The ZIF-8 shell in the nanoparticles is used to host doxorubicin (DOX) molecules for chemotherapy. At the same time, the g-C₃N₄ nanosheets are effective visible-light photosensitizer for PDT.⁴² Singlet oxygen can be generated upon photo-excitation and effectively transported out of the nanoparticles via the porous ZIF-8 shells. To the best of our knowledge, this is the first combinational therapy taking advantages of MOF structure and the approach shows much enhanced efficacy (Scheme 1b).



Scheme 1. Schematic illustration of core-shell nanoparticles and their combinational photo-chemo therapy. (a) Preparation of $g\text{-C}_3\text{N}_4@ZIF\text{-}8$ nanoparticles and drug loading. (b) Proposed mechanism of drug-loaded nanoparticles for fluorescence imaging and combination therapy.

2. Results and Discussion

2.1 Preparation and characterizations of $g\text{-C}_3\text{N}_4$ nanosheets

As metal-free semiconductors, $g\text{-C}_3\text{N}_4$ has been regarded as a suitable sustainable photocatalyst for facile preparation, abundant source, good stability and tunable electronic structure.^{43–47} Bulk $g\text{-C}_3\text{N}_4$ sheets of a few millimetres thick and several centimetres in diameter were first obtained from polymerization of melamine (Fig. S1a). X-ray photoelectron spectroscopy (XPS) shows that the bulk $g\text{-C}_3\text{N}_4$ composes mainly of N and C with a molar ratio of N:C of 1.29, close to stoichiometric 1.33 (Fig. S1d). Then $g\text{-C}_3\text{N}_4$ nanosheets were prepared by ultrasonic delamination of the bulk $g\text{-C}_3\text{N}_4$ sheets in water. Morphology of the $g\text{-C}_3\text{N}_4$ nanosheets was studied with atom force microscopy (AFM). As shown in Fig. 1a, the nanosheets have monodispersed size of about 30 nm and an average thickness of 4.5 nm (Fig. 1b). To demonstrate successful exfoliation, X-ray diffraction (XRD) and Fourier transform infrared (FTIR) spectroscopy were utilized to investigate the crystal and chemical structure of both the bulk and the nanosheets of $g\text{-C}_3\text{N}_4$. A FTIR spectrum of the $g\text{-C}_3\text{N}_4$ nanosheets shows the same vibration peaks (hydrogen bond and N-H stretching: $3000\text{--}3600\text{ cm}^{-1}$, C-NH-C stretching: $1000\text{--}1800\text{ cm}^{-1}$, triazine ring: 810 cm^{-1}) as the bulk materials, indicating the ultrasonic exfoliation has not changed their chemical structures (Fig. S3a). Fig. S3b shows that the characteristic (002) peak of $g\text{-C}_3\text{N}_4$ at 27.3° is much weaker in the nanosheet sample confirming successful exfoliation.⁴⁸ Fig. 1c is an HRTEM image of a nanosheet showing lattice fringes with spacing of 0.32 nm which matches well to that of the (002) plane of $g\text{-C}_3\text{N}_4$. Fig. 1d shows that the $g\text{-C}_3\text{N}_4$ nanosheets have an absorption peak at 315 nm and a photoluminescence (PL) peak at 455 nm. The inset of Fig. 1d is the pictures of $g\text{-C}_3\text{N}_4$

nanosheets under room and UV light. Under room light, it is a white uniform suspension. After exposure to UV light, the nanosheets present strong blue fluorescence.

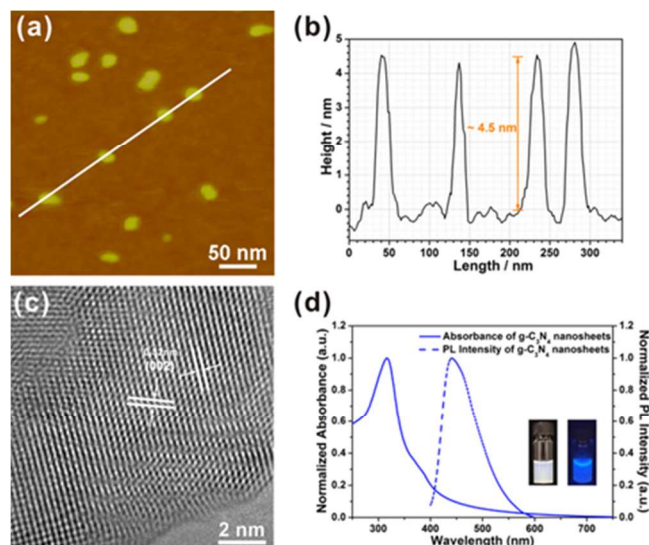


Fig. 1. Characterizations and properties of $g\text{-C}_3\text{N}_4$ nanosheets. (a) AFM topography of $g\text{-C}_3\text{N}_4$ nanosheets and (b) the corresponding height profile along the line in the image. (c) An HRTEM image of $g\text{-C}_3\text{N}_4$ nanosheets (d) Normalized UV-Vis absorbance (solid line) and photoluminescence spectra (dashed line) $g\text{-C}_3\text{N}_4$ nanosheets under excitation at 350 nm.

2.2 Preparation and characterizations of core-shell nanoparticles

For synthesis of core-shell nanoparticles with MOF shells, surface modifications on the cores (e.g., metal and protein) are typically required to stabilize the bare cores and increase their affinities to MOF precursors.^{49–53} However, this is not needed for encapsulating $g\text{-C}_3\text{N}_4$ nanosheets as they are negatively charged (Fig. S4a) and have excellent affinity to zinc ions. Therefore, this facilitates the simple synthesis of the $g\text{-C}_3\text{N}_4@ZIF\text{-}8$ core-shell nanoparticles and any additional surface modification of the $g\text{-C}_3\text{N}_4$ core is not required. It avoids the fluorescence of the $g\text{-C}_3\text{N}_4$ core being quenched by any surfactant. To construct core-shell nanoparticles, we employed a facile synthetic route by mixing precursors $\text{Zn}(\text{NO}_3)_2$, 2-methylimidazole (2-MIm) and $g\text{-C}_3\text{N}_4$ nanosheets in a methanol solution to grow the ZIF-8 shells surrounding the $g\text{-C}_3\text{N}_4$ nanosheets. SEM and TEM images of the products reveal that monodispersed spherical nanoparticles are prepared with an average size of about 60 nm (Fig. 2a, 2b). A high-magnification TEM image (Fig. 2c) confirms that the sample consists of $g\text{-C}_3\text{N}_4$ nanosheet of 30 nm in diameter encapsulated within ZIF nanoparticles. Fig. 2d shows an XRD pattern of the $g\text{-C}_3\text{N}_4@ZIF\text{-}8$ nanoparticles which is essentially the same as that of a pure ZIF-8 sample. The peak from the $g\text{-C}_3\text{N}_4$ nanosheet core is not observed. It is noted that, even in the pure $g\text{-C}_3\text{N}_4$ nanosheet sample, its peak is weak (Fig. S3b). The absence of the $g\text{-C}_3\text{N}_4$ peak in the $g\text{-C}_3\text{N}_4@ZIF\text{-}8$ core-shell nanoparticles is also attributed to the small volume fraction of the nanosheets.

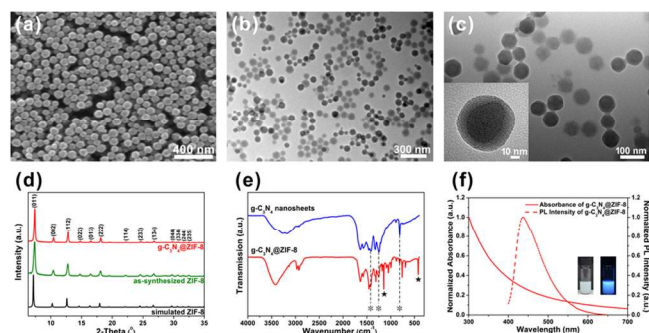


Fig. 2. Characterizations and properties of $g\text{-C}_3\text{N}_4@ZIF\text{-}8$ nanoparticles. (a) SEM image of as-prepared nanoparticles. (b), (c) TEM image of as-prepared nanoparticles under different magnification. (d) XRD diffraction of $g\text{-C}_3\text{N}_4@ZIF\text{-}8$ (red), ZIF-8 nanospheres (green), simulated ZIF-8 (black). (e) FTIR spectra of $g\text{-C}_3\text{N}_4$ nanosheets (blue) and $g\text{-C}_3\text{N}_4@ZIF\text{-}8$ (red). (f) Normalized UV-Vis absorbance (solid line) and photoluminescence spectra (dash line) of $g\text{-C}_3\text{N}_4@ZIF\text{-}8$ with excitation at 350 nm.

While the XRD pattern of the core-shell nanoparticles does not show the existence of $g\text{-C}_3\text{N}_4$ nanosheets, the $g\text{-C}_3\text{N}_4$ phase can be confirmed with FTIR. Fig. 2e is a representative FTIR spectrum of the $g\text{-C}_3\text{N}_4@ZIF\text{-}8$ nanoparticles which shows characteristics from both $g\text{-C}_3\text{N}_4$ (marked with *) and ZIF-8 (marked with ★).⁵⁴ Dynamic light scattering (DLS) measurements show that in contrast to the negative charge on the pure $g\text{-C}_3\text{N}_4$ nanosheets (Fig. S3a), zeta potential of the as-prepared $g\text{-C}_3\text{N}_4@ZIF\text{-}8$ nanoparticles is +31.9 mV (Fig. S3b) which is similar to that of the pure ZIF-8.⁵⁵ As illustrated in Fig. 2f, the $g\text{-C}_3\text{N}_4@ZIF\text{-}8$ nanoparticles shows a PL spectrum almost identical to that of the pure $g\text{-C}_3\text{N}_4$ further confirming the existence of the $g\text{-C}_3\text{N}_4$ phase. The inset of Fig. 2f displays the pictures of the core-shell nanoparticles under room and UV light. Under room light, the sample is still a white uniform suspension. After exposure to UV light, the suspension remains the blue fluorescence of the $g\text{-C}_3\text{N}_4$ nanosheets.

2.3 Singlet oxygen detection

The capability of the $g\text{-C}_3\text{N}_4@ZIF\text{-}8$ nanoparticles for singlet oxygen generation was evaluated with the standard singlet oxygen sensor green (SOSG) probe. With reaction of $^1\text{O}_2$, the intramolecular electron transfer within SOSG is prohibited, which recovers the quenched green fluorescence with high selectivity.^{56, 57} As shown in Fig. 3a, when the mixture of SOSG and $g\text{-C}_3\text{N}_4@ZIF\text{-}8$ nanoparticles is irradiated with visible light, the fluorescence intensity of SOSG at 530 nm exhibits time-dependent increase, indicating the gradual generation of $^1\text{O}_2$. Fig. 3b illustrates the change in SOSG's fluorescence intensity incubated with pure $g\text{-C}_3\text{N}_4$ nanosheets, pure ZIF-8 nanoparticles and $g\text{-C}_3\text{N}_4@ZIF\text{-}8$ core-shell nanoparticles. For pure ZIF-8 (same weight of ZIF-8 as in the core-shell nanoparticle), the fluorescence intensity of SOSG is constantly low under irradiation, indicating that the ZIF-8 shells does not generate $^1\text{O}_2$. In comparison, the fluorescence intensity of SOSG shows similar increase with time in the presence of pure $g\text{-C}_3\text{N}_4$ nanosheets and $g\text{-C}_3\text{N}_4@ZIF\text{-}8$ nanoparticles. These results suggest that (1) the singlet oxygen be predominantly generated by $g\text{-C}_3\text{N}_4$ phase and (2) the singlet oxygen generated in the $g\text{-C}_3\text{N}_4$ core of the $g\text{-C}_3\text{N}_4@ZIF\text{-}8$

nanoparticles effectively diffuse out. Overall, this demonstrates a good potential for application as a PDT agent.

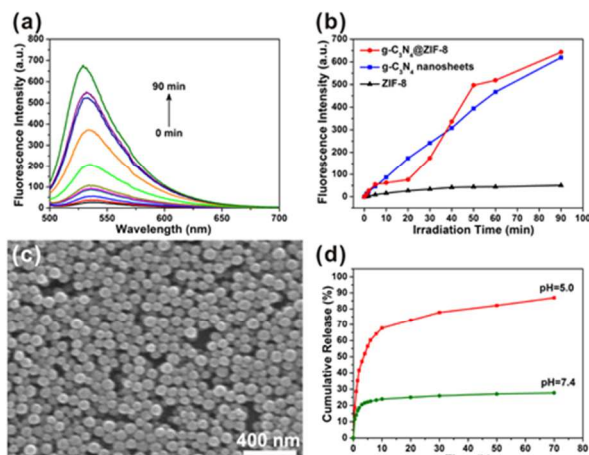


Fig. 3. (a) Fluorescence spectra of SOSG solution incubated with $g\text{-C}_3\text{N}_4@ZIF\text{-}8$ over increasing irradiation time. (b) The evolution of the fluorescence intensity of SOSG at 530 nm over different irradiation times. (c) SEM image of DOX-loaded $g\text{-C}_3\text{N}_4@ZIF\text{-}8$ nanoparticles. (d) Release profile of DOX from drug-loaded $g\text{-C}_3\text{N}_4@ZIF\text{-}8$ in simulated physiological solution with pH values of 5.0 and 7.4.

2.4 pH-sensitive drug release profiles

To further endow $g\text{-C}_3\text{N}_4@ZIF\text{-}8$ nanoparticles with ability of chemotherapy, the nanoparticles were soaked in a 1 mg/mL doxorubicin (DOX) solution at a weight ratio of 1:1 (optimized as shown in Table S1) for 2 days. The loading efficiency is about 35% with a saturated loading content of about 0.336 mg of DOX for 1 mg of nanoparticles as determined by UV-Vis absorption. After drug loading, the nanoparticles show neither observable size increase nor any sign of dissociation (Fig. 3c). Drug-release experiments were carried out in phosphate buffer solutions of two different pH values. In Fig. 3d, DOX-loaded $g\text{-C}_3\text{N}_4@ZIF\text{-}8$ nanoparticles exhibit progressive release without any burst dissociation. When immersed in pH 7.4 buffer, only around 25% of loaded DOX was released into the ambient solution after 70 hours. In comparison, the delivery of DOX reveals enhanced effect with about 85% of cargo released at a pH value of 5.0 within the same period. The pH-sensitive release profile attributes to the acid-promoted dissolution of ZIF-8 which is previously reported in ZIF-8 systems.^{58, 59} These results show that a pH-sensitive drug release profile can be realized with the present $g\text{-C}_3\text{N}_4@ZIF\text{-}8$ cores-shell nanoparticles, which is beneficial for targeted drug release at acidic tumour sites.²⁷

2.5 Dual-color fluorescence imaging of DOX-loaded nanoparticles

To investigate the cellular localization of $g\text{-C}_3\text{N}_4@ZIF\text{-}8$ nanoparticles, human alveolar cancer cells A549 were individually incubated with pure DOX (5 $\mu\text{g}/\text{mL}$) and $g\text{-C}_3\text{N}_4@ZIF\text{-}8$ nanoparticles (and 25 $\mu\text{g}/\text{mL}$) with or without DOX loading. In the control group, pristine A549 cells do not show any fluorescent signal (Fig. 4a). For the group incubating with nanoparticles without DOX (Fig. 4b), the subcellular blue

fluorescence confirms the endocytosis of the $g\text{-C}_3\text{N}_4\text{@ZIF-8}$ nanoparticles into the cytoplasm. In comparison, free DOX molecules with red fluorescent signal tend to accumulate in the nuclei as shown in Fig. 4c.⁶⁰ For the cells incubated with DOX-loaded nanoparticles (Fig. 4d), the nuclei are full of the red fluorescence from DOX and surrounded by the blue fluorescence from the $g\text{-C}_3\text{N}_4$ nanosheets in cytoplasm. These results indicate that the DOX-loaded $g\text{-C}_3\text{N}_4\text{@ZIF-8}$ nanoparticles can effectively deliver DOX into the cell nucleus and provide dual-colour fluorescence imaging.

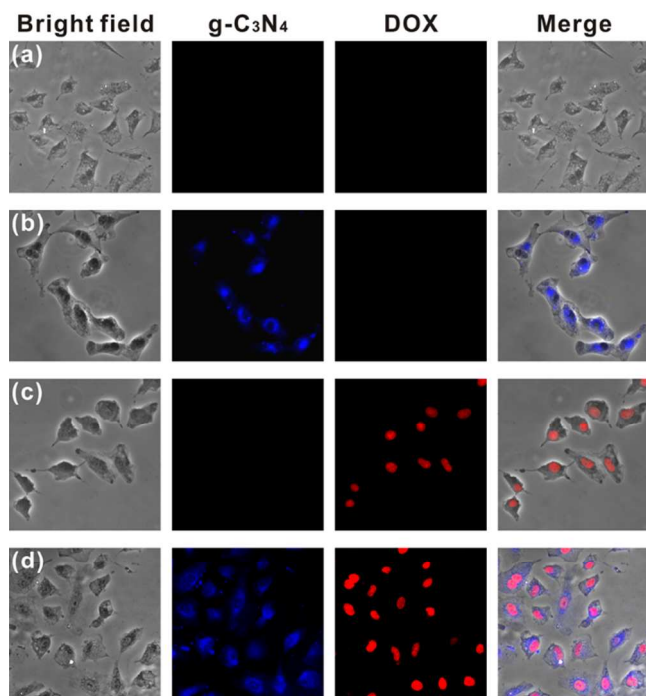


Fig. 4. Optical microscopy images of A549 cells under different conditions: (a) untreated, (b) incubated with 25 $\mu\text{g/mL}$ of $g\text{-C}_3\text{N}_4\text{@ZIF-8}$ nanoparticles, (c) treated with 5 $\mu\text{g/mL}$ of DOX, and (d) incubated with 25 $\mu\text{g/mL}$ of DOX-loaded nanoparticles. The left column shows the bright field images. The central 2 columns are the fluorescence images of $g\text{-C}_3\text{N}_4$ and DOX channels. The right column presents the overlay images of the bright field and fluorescence images. The fluorescent images were taken by fluorescent microscopy under an excitation range of 330–380 nm and 450–490 nm for nanoparticle and DOX channel, respectively.

2.6 *In vitro* cytotoxicity evaluation

To evaluate the feasibility of our core-shell system for combination therapy, the cytotoxicity of $g\text{-C}_3\text{N}_4\text{@ZIF-8}$ nanoparticles with or without DOX loading were analysed with the 3-(4,5-dimethylthiazol-2-yl)-2,5-diphenyltetrazolium bromide (MTT) assay in A549 cell line in dark or under visible light irradiation. Pure $g\text{-C}_3\text{N}_4$ nanosheets show negligible cytotoxicity under the condition of no light irradiation (Fig. S5). It can be seen from Fig. 5a that the viability of the tumour cells incubated with $g\text{-C}_3\text{N}_4\text{@ZIF-8}$ nanoparticles without DOX (green) is almost the same as that of the control group (cell irradiated with visible light only, i.e. without nanoparticle). This demonstrates the excellent biocompatibility of the as-prepared core-shell nanoparticles. When incubated

with the DOX-loaded nanoparticles in dark (red), the death of A549 cell obviously increases with nanoparticle concentrations. On the other hand, $g\text{-C}_3\text{N}_4\text{@ZIF-8}$ nanoparticles without DOX (blue) can also effectively kill cells under visible light irradiation, confirming their PDT effect. The highest cell-killing rate is achieved with the combined action of DOX and irradiation (magenta), when cells are incubated with DOX-loaded nanoparticles under irradiation. For example, the cell viability of DOX-loaded nanoparticles under irradiation is 16.6% at 100 $\mu\text{g/mL}$ concentration, which shows much more cytotoxicity than that of 40.3% in the DOX-loaded nanoparticles group and that of 44.9% in the irradiated nanoparticles group at the same concentration. Furthermore, the combinational therapeutic effect of $g\text{-C}_3\text{N}_4\text{@ZIF-8}$ nanoparticles was also observed with calcein AM and ethidium homodimer-1 co-staining. In Fig. 5b, the pristine cells with exposure to visible irradiation for 15 minutes display only green fluorescence, indicating that the irradiation does not induce cell death. However, the cells incubated with DOX-loaded nanoparticles are almost all killed after identical irradiation. These results are in good agreement with those from the MTT assay, which confirms the combined therapies of $g\text{-C}_3\text{N}_4\text{@ZIF-8}$ nanoparticles can effectively destroy cancer cells. Collectively, these results suggest that the DOX-loaded $g\text{-C}_3\text{N}_4\text{@ZIF-8}$ nanosheet@ZIF-8 core-shell nanoparticles can act as a robust therapeutic agent to achieve dual-colour fluorescence imaging and synergic photodynamic-chemo therapy.

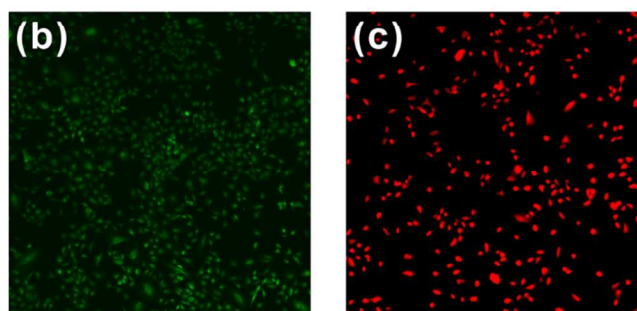
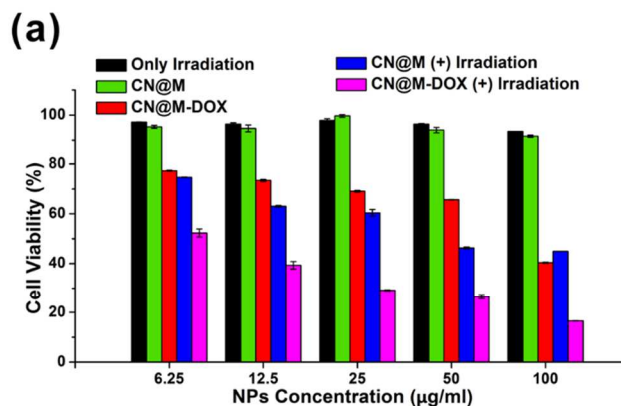


Fig. 5. (a) A549 cell viabilities at different concentrations of $g\text{-C}_3\text{N}_4\text{@ZIF-8}$ (CN@M), DOX-loaded $g\text{-C}_3\text{N}_4\text{@ZIF-8}$ (CN@M-DOX) for 24 h at 37 $^{\circ}\text{C}$ with or without 15-min irradiation of visible light (100 mW/cm^2). Fluorescence images of calcein AM and ethidium homodimer-1 co-stained A549 cancer cells incubated (b) without any nanoparticles, (c) with DOX-loaded $g\text{-C}_3\text{N}_4\text{@ZIF-8}$ for 24 h at 37 $^{\circ}\text{C}$ after irradiation.

3. Conclusions

In summary, we designed and developed a novel nanoscaled core-shell platform composing DOX-loaded $g\text{-C}_3\text{N}_4@\text{ZIF-8}$ nanoparticles for combinational chemo-therapy and photodynamic therapy. The prepared $g\text{-C}_3\text{N}_4@\text{ZIF-8}$ nanoparticles possess good biocompatibility and can efficiently generate singlet oxygen. The nanoparticles can be loaded with an anticancer drug of DOX and deliver the drug with a preferred pH-sensitive release profile. Furthermore, DOX-loaded $g\text{-C}_3\text{N}_4@\text{ZIF-8}$ nanoparticles, as multifunctional nanoscale platform, are effective for dual-colour fluorescence imaging and imaging-guided photo-chemo therapy upon tumour cells. We anticipate that the integration of functional nanomaterials and MOF shells into core-shell nanostructures would offer a promising pathway to construct enhanced combinational therapeutics for clinical cancer treatment in the near future.

4. Experimental

4.1 Materials

Melamine ($\text{C}_3\text{H}_4\text{N}_6$, 99%), zinc nitrate hexahydrate ($\text{Zn}(\text{NO}_3)_2 \cdot 6\text{H}_2\text{O}$, 99%), doxorubicin hydrochloride (DOX), 2-methyl imidazole ($\text{C}_4\text{H}_6\text{N}_2$, 99%), methanol (ACS grade, 99%), and phosphate citrate buffer were purchased from Sigma-Aldrich. Singlet Oxygen Sensor Green Reagent was ordered from Life Technology. High-purity water with a resistivity greater than $18.4 \text{ M}\Omega\text{-cm}$ was collected from an in-line Millipore RiOs/Origin water purification system. Unless otherwise noted, all chemicals were used without further purification.

4.2 Synthesis of $g\text{-C}_3\text{N}_4$ nanosheets

Bulk $g\text{-C}_3\text{N}_4$ was prepared by polymerization of melamine in a semi-closed system. Typically, melamine (5 g) in a crucible was heated at $600 \text{ }^\circ\text{C}$ for 2 h with a heating and cooling ramp rate of $3 \text{ }^\circ\text{C}/\text{min}$. The obtained bulk $g\text{-C}_3\text{N}_4$ product was yellow powder. A liquid exfoliating method was employed to obtain $g\text{-C}_3\text{N}_4$ nanosheets. Briefly, bulk $g\text{-C}_3\text{N}_4$ powder (40 mg) was dispersed in water (40 mL) under ultrasonication (300W) for about 14 hours. The initial light-yellow suspension was then centrifuged at 5000 rpm to remove unexfoliated bulk $g\text{-C}_3\text{N}_4$, which resulted in a lightly milky suspension of $g\text{-C}_3\text{N}_4$ nanosheets. The concentration of $g\text{-C}_3\text{N}_4$ nanosheets is about 0.15 mg/mL by weighing dried samples. To improve the size distribution of $g\text{-C}_3\text{N}_4$ nanosheets as a suitable core material, the exfoliated $g\text{-C}_3\text{N}_4$ milky solution was further centrifuged at 7000 rpm and the supernatant was concentrated from 10 mL to 1 mL of aqueous solution.

4.3 Synthesis of $g\text{-C}_3\text{N}_4@\text{ZIF-8}$ core-shell nanoparticles

Zinc nitrate hexahydrate (150 mg) and 2-methyl imidazole (350 mg) were dissolved in methanol (7.2 mL). Subsequently, 1 mL of the concentrated $g\text{-C}_3\text{N}_4$ nanosheets in water was added into the zinc nitrate solution followed by 5-min agitation. Then, 2-methyl imidazole solution was injected into the jar while stirring continuously for another 5 min. The reaction solution became milky gradually, indicating the formation of ZIF-8 shells. Then the formed nanoparticles were washed with 15 mL of methanol for three times and then centrifuged at 7000 rpm for 15 min to obtain the precipitation of ZIF-8 nanoparticles. For the last step, white $g\text{-C}_3\text{N}_4@\text{ZIF-8}$ core-shell nanoparticles

were suspended into methanol (5 mL) for storage with the concentration of 5 mg/mL .

4.3 Characterizations

Scanning electron microscopy was carried on JEOL JSM-820 scanning electron microscope. Energy disperse X-ray (EDX) equipment is attached to SEM. Besides, transmission electron microscopy images were obtained with a Philips CM-20 or a CM-200FEG transmission electron microscope. X-ray photoelectron spectra was obtained by Physical Electronics PHI5802 with Al mono excitation source ($h\nu = 1486.6 \text{ eV}$). Powder X-ray diffraction was recorded with a Siemens D500 X-Ray Diffractometer with Cu $K\alpha$ radiation source ($\lambda = 1.5406 \text{ \AA}$). Fourier transform infrared spectra were obtained on Perkin-Elmer Spotlight 100 in a KBr pellet, scanning from 4000 to 400 cm^{-1} . Atomic force microscopy was performed with a Veeco Multimode-V. Dynamic light scattering was conducted on a Malvern Zetasizer Nano ZS instrument. Ultraviolet-visible light absorption and photoluminescence were recorded with a Cary 50Conc UV-Visible spectrophotometer and a Cary Eclipse fluorescence spectrophotometer respectively. All irradiation came from a Newport Solar Simulator with filters to get irradiation wavelength from 400 to 700 nm.

4.4 Singlet oxygen detection

To evaluate the generation of singlet oxygen, Singlet Oxygen Sensor Green (SOSG) was chosen for $g\text{-C}_3\text{N}_4@\text{ZIF-8}$ nanoparticles system. Specifically, the SOSG was mixed with $100 \text{ }\mu\text{g}$ of nanoparticles at a final concentration of $10 \text{ }\mu\text{M}$. The control groups were the $g\text{-C}_3\text{N}_4$ nanosheets and as-synthesized ZIF-8 nanoparticles with same weight of those as in the core-shell nanoparticles during synthesis. The mixture solutions were irradiated with visible light at an intensity of $100 \text{ mW}/\text{cm}^2$ for different durations from 0 to 90 minutes. Photoluminescent spectra of the irradiated samples were then measured with an excitation source of 490 nm to determine the fluorescent intensity of SOSG. The singlet oxygen generation of samples was quantified by comparing the fluorescence enhancement with the control groups.

4.5 Drug loading and release

In order to evaluate drug-loading capacity of $g\text{-C}_3\text{N}_4@\text{ZIF-8}$ nanoparticle, 5 mg of nanoparticles was dispersed in 5 mL of DOX aqueous solution with the concentration of 1 mg/mL under ultrasonication. The mixture of drug and nanoparticles was stirred for 2 days and then collected through centrifugation. The concentration of DOX in the supernatant was determined by the absorbance of DOX at 480 nm. Then the drug loading efficiency and content were calculated.

For drug release experiments, the obtained DOX-loaded nanoparticles were directly soaked in 5 mL of solutions with pH values of 7.4 and 5.0. The system was kept in $37 \text{ }^\circ\text{C}$ with a gentle shake. The supernatant was collected by centrifugation and determined by UV-Vis spectroscopy to calculate the amount of released DOX at specific time.

4.6 Dual-color fluorescence imaging

To confirm the imaging function of drug-loaded nanoparticles, $200 \text{ }\mu\text{L}$ of $100 \text{ }\mu\text{g/mL}$ DOX-loaded nanoparticles was added into $800 \text{ }\mu\text{L}$ of cell medium containing A549 cells. After 4-hour

incubation, fluorescent images were taken by fluorescent microscopy under an excitation range of 330-380 nm and 450-490 nm.

4.7 *In vitro* photo-chemo therapy

The cytotoxicity of g-C₃N₄@ZIF-8 nanoparticles was evaluated by standard 3-(4,5-dimethylthiazol-2-yl)-2,5-diphenyltetrazolium bromide (MTT) assay in A549 cell line. A549 cells were seeded and incubated at 37 °C in Dulbecco's modified Eagles medium (DMEM) containing 10% fetal bovine serum (FBS) under an atmosphere of 5% CO₂ for one day. Then, g-C₃N₄@ZIF-8 nanoparticles and DOX-loaded nanoparticles were added individually into different groups of cells. When incubated for 12 h, light groups are irradiated under Xenon lamp for 15 min. After an incubation time of 24 h under standard conditions, a certain amount of MTT solution in PBS (pH=7.4) was added and incubated for another 4 h. The medium was removed by DMSO while shaking. After that, a micro-plate reader was used to measure the absorbance at 490 nm. Furthermore, to avoid random error, every group with a certain drug concentration was tested five times.

Notes and references

a Center of Super-Diamond and Advanced Films (COSDAF) & Department of Physics and Materials Science, City University of Hong Kong, Hong Kong SAR, P. R. China.

b School of Chemistry and Forensic Sciences, Faculty of Life Sciences, University of Bradford, United Kingdom

*Corresponding author.

E-mail: xianfeng_chen@hotmail.com

E-mail: apcslee@cityu.edu.hk

Electronic Supplementary Information (ESI) available: [details of any supplementary information available should be included here]. See DOI: 10.1039/b000000x/

- 1 J. L. C. Rowsell, A. R. Millward, K. S. Park, O. M. Yaghi, *J. Am. Chem. Soc.* 2004, **126**, 5666.
- 2 H. Hayashi, A. P. Cote, H. Furukawa, M. O'Keefe, O. M. Yaghi, *Nat. Mater.* 2007, **6**, 501.
- 3 P. L. Llewellyn, S. Bourrelly, C. Serre, A. Vimont, M. Daturi, L. Hamon, G. De Weireld, J. Chang, D. Hong, Y. K. Hwang, S. H. Jung, G. Ferey, *Langmuir* 2008, **24**, 7245.
- 4 G. Li, H. Kobayashi, J. M. Taylor, R. Ikeda, Y. Kubota, K. Kato, M. Takata, T. Yamamoto, S. Toh, S. Matsumura, H. Kitagawa, *Nat. Mater.* 2014, **13**, 802.
- 5 J. S. Seo, D. Whang, H. Lee, S. I. Jun, J. Oh, Y. J. Jeon, K. Kim, *Nature* 2000, **404**, 982.
- 6 C. Wang, Z. Xie, K. E. deKrafft, W. Lin, *J. Am. Chem. Soc.* 2011, **133**, 13445.
- 7 X. Huang, Y. Chen, Z. Lin, X. Ren, Y. Song, Z. Xu, X. Dong, X. Li, C. Hu, B. Wang, *Chem. Comm.* 2014, **50**, 2624.
- 8 W. Cho, H. J. Lee, G. Choi, S. Choi, M. Oh, *J. Am. Chem. Soc.* 2014, **136**, 12201.
- 9 C. He, K. Lu, W. Lin, *J. Am. Chem. Soc.* 2014, **136**, 12253.
- 10 S. T. Meek, J. A. Greathouse, M. D. Allendorf, *Adv. Mater.* 2011, **23**, 249.
- 11 J. Li, J. Sculley, H. Zhou, *Chem. Rev.* 2012, **112**, 869.
- 12 M. Eddaoudi, J. Kim, N. Rosi, D. Vodak, J. Wachter, M. O'Keefe, O. Yaghi, *Science* 2002, **295**, 469.
- 13 J. L. C. Rowsell, O. M. Yaghi, *Micropor. Mesopor. Mater.* 2004, **73**, 3.
- 14 K. K. Tanabe, Z. Wang, S. M. Cohen, *J. Am. Chem. Soc.* 2008, **130**, 8508.
- 15 C. Wang, D. Liu, W. Lin, *J. Am. Chem. Soc.* 2013, **135**, 13222.
- 16 X. Liang, X. Li, X. Yue, Z. Dai, *Angew. Chem. Int. Ed.* 2011, **50**, 11622.
- 17 X. Xu, R. Cao, S. Jeong, J. Cho, *Nano Lett.* 2012, **12**, 4988.
- 18 S. Horike, D. Umeyama, S. Kitagawa, *Acc. Chem. Res.* 2013, **46**, 2376.
- 19 K. Lu, C. He, W. Lin, *J. Am. Chem. Soc.* 2014, **136**, 16712.
- 20 J. D. Rocca, D. Liu, W. Lin, *Acc. Chem. Res.* 2011, **44**, 957.
- 21 S. Keskin, S. Kizilel, *Ind. Eng. Chem. Res.* 2011, **50**, 1799.
- 22 A. C. McKinlay, R. E. Morris, P. Horcajada, G. Ferey, R. Gref, P. Couvreur, C. Serre, *Angew. Chem. Int. Ed.* 2010, **49**, 6260.
- 23 P. Horcajada, R. Gref, T. Baati, P. K. Allan, G. Maurin, P. Couvreur, G. Ferey, R. E. Morris, C. Serre, *Chem. Rev.* 2012, **112**, 1232.
- 24 C. Tamames-Tabar, D. Cunha, E. Imbuluzqueta, F. Ragon, C. Serre, M. J. Blanco-Prieto, P. Horcajada, *J. Mater. Chem. B* 2014, **2**, 262.
- 25 P. Horcajada, C. Serre, M. Vallet-Regi, M. Sebban, F. Taulelle, G. Ferey, *Angew. Chem. Int. Ed.* 2006, **45**, 5974.
- 26 P. Horcajada, T. Chalati, C. Serre, B. Gillet, C. Sebrie, T. Baati, J. F. Eubank, D. Heurtaux, P. Clayette, C. Kreuz, J. Chang, Y. K. Hwang, V. Marsaud, P. Bories, L. Cynober, S. Gil, G. Ferey, P. Couvreur, R. Gref, *Nat. Mater.* 2010, **9**, 172.
- 27 C. Sun, C. Qin, C. Wang, Z. Su, S. Wang, X. Wang, G. Yang, K. Shao, Y. Lan, E. Wang, *Adv. Mater.* 2011, **23**, 5629.
- 28 J. B. Fitzgerald, B. Schoeberl, U. B. Nielsen, P. K. Sorger, *Nat. Chem. Biol.* 2006, **2**, 458.
- 29 K. J. Son, H. Yoon, J. Kim, W. Jang, Y. Lee, W. Koh, *Angew. Chem. Int. Ed.* 2011, **50**, 11968.
- 30 C. He, K. Lu, D. Liu, W. Lin, *J. Am. Chem. Soc.* 2014, **136**, 5181.
- 31 G. Canti, A. Nicolini, R. Cubeddu, P. Taroni, G. Bandieramonte, G. Valentini, *Cancer Lett.* 1998, **125**, 39.
- 32 M. Zuluaga, N. Lange, *Curr. Med. Chem.* 2008, **15**, 1655.
- 33 C. Peng, P. Lai, F. Lin, S. Y. Wu, M. Shieh, *Biomaterials* 2009, **30**, 3614.
- 34 J. T. F. Lau, P. Lo, W. Fong, D. K. P. Ng, *J. Med. Chem.* 2012, **55**, 5446.
- 35 Y. Yuan, B. Liu, *ACS Appl. Mater. Inter.* 2014, **6**, 14903.
- 36 C. He, D. Liu, W. Lin, *ACS Nano* 2015, **9**, 991.
- 37 Y. Chen, Q. Xu, S. Yu, H. Jiang, *Small* 2014, **11**, 71.
- 38 L. Lin, T. Zhang, H. Liu, J. Qiu, X. Zhang, *Nanoscale* 2015, **7**, 7615.
- 39 M. Zhao, K. Deng, L. He, Y. Liu, G. Li, H. Zhao, Z. Tang, *J. Am. Chem. Soc.* 2014, **136**, 1738.
- 40 K. Deng, Z. Hou, X. Li, C. Li, Y. Zhang, X. Deng, Z. Cheng, J. Lin, *Sci. Rep.* 2015, **5**, 7851.
- 41 Y. Li, J. Tang, L. He, Y. Liu, Y. Liu, C. Chen, Z. Tang, *Adv. Mater.* 2015, DOI: 10.1002/adma.201501779.
- 42 L. Lin, Z. Cong, J. Li, K. Ke, S. Guo, H. Yang, G. Chen, *J. Mater. Chem. B* 2014, **2**, 1031.
- 43 X. Wang, K. Maeda, A. Thomas, K. Takanabe, G. Xin, J. M. Carlsson, K. Domen, M. Antonietti, *Nat. Mater.* 2009, **8**, 76.
- 44 C. L. Schmidt, M. Jansen, *J. Mater. Chem.* 2010, **20**, 4183.
- 45 Y. Wang, X. Wang, M. Antonietti, *Angew. Chem. Int. Ed.* 2012, **51**, 68.
- 46 S. Cao, J. Low, J. Yu, M. Jaroniec, *Adv. Mater.* 2015, **27**, 2150.

- 47 Z. Zhao, Y. Sun, F. Dong, *Nanoscale* 2015, **7**, 15.
- 48 P. Niu, L. Zhang, G. Liu, H. Cheng, *Adv. Funct. Mater.* 2012, **22**, 4763.
- 49 S. Yang, Y. Gong, J. Zhang, L. Zhan, L. Ma, Z. Fang, R. Vajtai, X. Wang, P. M. Ajayan, *Adv. Mater.* 2013, **25**, 2452.
- 50 G. Lu, S. Li, Z. Guo, O. K. Farha, B. G. Hauser, X. Qi, Y. Wang, X. Wang, S. Han, X. Liu, J. S. DuChene, H. Zhang, Q. Zhang, X. Chen, J. Ma, S. C. J. Loo, W. D. Wei, Y. Yang, J. T. Hupp, F. Huo, *Nat. Chem.* 2012, **4**, 310.
- 51 Y. Liu, Z. Tang, *Adv. Mater.* 2013, **25**, 5819.
- 52 F. Lyu, Y. Zhang, R. N. Zare, J. Ge, Z. Liu, *Nano Letters.* 2014, **14**, 5761.
- 53 W. Zhang, G. Lu, C. Cui, Y. Liu, S. Li, W. Yan, C. Xing, Y. R. Chi, Y. Yang, F. Huo, *Adv. Mater.* 2014, **26**, 4056.
- 54 C. Sun, C. Qin, X. Wang, G. Yang, K. Shao, Y. Lan, Z. Su, P. Huang, C. Wang, E. Wang, *Dalton Trans.* 2012, **41**, 6906.
- 55 J. Zhuang, C. Kuo, L. Chou, D. Liu, E. Weerapana, C. Tsung, *ACS Nano* 2014, **8**, 2812.
- 56 P. Huang, J. Lin, X. Wang, Z. Wang, C. Zhang, M. He, K. Wang, F. Chen, Z. Li, G. Shen, D. Cui, X. Chen, *Adv. Mater.* 2012, **24**, 5104.
- 57 J. Lin, S. Wang, P. Huang, Z. Wang, S. Chen, G. Niu, W. Li, J. He, D. Cui, G. Lu, X. Chen, Z. Nie, *ACS Nano* 2013, **7**, 5320.
- 58 H. Ren, L. Zhang, J. An, T. Wang, L. Li, X. Si, L. He, X. Wu, C. Wang, Z. Su, *Chem. Comm.* 2014, **50**, 1000.
- 59 I. B. Vasconcelos, T. G. da Silva, G. C. G. Militao, Th. A. Soares, N. M. Rodrigues, M. O. Rodrigues, N. B. da C. Jr., R. O. Freiree, S. A. Junior, *RSC Adv.* 2012, **2**, 9437.
- 60 X. Xiong, Z. Ma, R. Lai, A. Lavasanifar, *Biomaterials* 2010, **30**, 757.